Available online at www.sciencedirect.com
ScienceDirect
Procedia Engineering 2 (2010) 265–273
Procedia Engineering
www.elsevier.com/locate/procedia

Fatigue 2010

Dynamic strain ageing and dynamic precipitation in AA7030 during cyclic deformation

Magnus Hörnqvist[a,b,*], Birger Karlsson[a]

[a]Chalmers University of Technology, Materials and Manufacturing Technology, Gothenburg, S-41296, Sweden
[b]Presently at Materials Technology, Volvo Aero Corporation Trollhättan, S-46181, Sweden

Received 26 February 2010; revised 9 March 2010; accepted 15 March 2010

Abstract

The effects of dynamic strain ageing (DSA) and dynamic precipitation (DP) on the stress–strain response during low-cycle fatigue of naturally aged (NA) and peak-aged (PA) AA7030 alloy at different temperatures was investigated. The results show that the PA temper is largely unaffected by DSA/DP, and the cyclic deformation behavior is controlled by the accumulation of dislocations and strain localization due to repeated shearing of precipitates. In the NA temper, on the other hand, the effect of temperature on DSA and DP is the main mechanism controlling the stress–strain response. At temperature above room temperature, DP in the intense slip bands inhibits cyclic softening and the samples harden until the on-set of crack growth. At lower temperatures, the rate of DP is too slow to compensate for the softening in the slip bands and the stress amplitude saturates or decreases. The stress amplitude development is shown to primarily be a result of the evolution of the effective stress associated with dislocation–precipitate interactions.

Keywords: Al-Zn-Mg; Low-cycle fatigue; Cyclic deformation; Dynamic precipitation; Dynamic strain ageing.

1. Introduction

The effects of dynamic strain ageing (DSA), where mobile solute atoms repeatedly lock moving dislocations, thereby causing increased flow stresses, reduced ductility, negative strain rate sensitivity, positive temperature sensitivity etc., are well known under monotonic deformation of aluminium alloys. The alloy AA7030 has been shown earlier to exhibit strong DSA effects in naturally aged [1-3] and solution treated [4-8] conditions, while weak effects were found in the peak-aged material [1-3,8].

Dynamic precipitation (DP) occurs readily under monotonic plastic deformation of supersaturated 7000 series aluminium alloys [9-12]. The phenomenon of DP is closely related to DSA, where the initial solute clustering required for precipitation is caused by the DSA of dislocation junctions. When the dislocations break free from the solute lock, the clusters left behind can nucleate precipitates which act as obstacles for the following dislocations [11]. This causes a continuous increase in the flow stress, which can be seen as an additional strain hardening in

* Corresponding author. Tel.: +46-520-94074; fax: +46-520-98589.
E-mail address: magnus.hornqvist@volvo.com.

1877-7058 © 2010 Published by Elsevier Ltd.
doi:10.1016/j.proeng.2010.03.029

Nomenclature

A	asymmetry factor
DP	dynamic precipitation
DSA	dynamic strain ageing
N	cycle number
N_f	number of cycles to failure
NA	naturally aged (temper)
PA	peak-aged (temper)
ε	true strain
ε_a	strain amplitude
$\varepsilon_{a,p}$	plastic strain amplitude
σ	true stress
σ_a	stress amplitude
σ_c	compressive peak stress
σ_{eff}	effective stress
$\sigma_{eff,prec}$	precipitate contribution to the effective stress
σ_{int}	internal stress
σ_m	mean stress
σ_t	tensile peak stress

monotonic deformation [9-14]. For solution treated Al-Zn-Mg it has been reported that DP occurs through nucleation of small (0.6 nm) zones, while in naturally aged material the main effect is growth if existing zones (in the range of 1 nm) [11]. Indirect observations of precipitation of clusters, invisible in electron microscopy, during plastic flow of a Al-Zn-Mg alloy in the DSA regime have been made [15].

The occurrence of DP during cyclic plastic deformation of aluminium alloys is so far largely unexplored. Christ *et al*. [16] showed that a solution treated Al-Zn-Mg-Cu alloy, corresponding to AA7022, showed extensive cyclic hardening and drastically reduced fatigue life under low-cycle fatigue conditions, and this was shown to be a result of dynamic precipitation during cycling. Cyclically deformed Al-Ag alloys, heat treated to contain Guinier-Preston (GP) zones and shearable γ' precipitates, showed evidence of deformation induced precipitation of stable phases, and even over-ageing [17,18]. In the process, the GP zones in the vicinity of the precipitates dissolved. However, the precise effects of the precipitation during cycling on the cyclic stress–strain response were not clearly revealed [17]. Al-Cu alloys aged to contain GP zones and θ'', on the other hand, did not show any trace of deformation induced precipitation [19].

In previous investigations it was shown that naturally aged AA7030 cyclically hardens until the on-set of crack growth, in spite of strong strain localization [20]. Normally, the repeated localization of strain into slip bands as a result of precipitate shearing leads to a softening during cycling [21-23], as was observed in the peak-aged version of the same alloy [20]. One explanation for this anomalous behavior could be that DP occurs during cycling, which continuously increases the flow stress level. This paper aims to further investigate the connection between cyclic plastic deformation and concomitant DSA and DP through indirect observations during LCF testing at different temperatures of AA7030 in different tempers.

2. Experimental

The material was obtained in the form of extruded rods, 36 mm in diameter, with a grain size of approximately 120 μm. Cylindrical samples, with a waist diameter of 10 mm and a parallel length of 16 mm, were machined from the rods. The material was solution treated at 480ºC for 30 min, water quenched and aged 24 h at room temperature to obtain the temper referred to as the *naturally aged* (NA). For comparison, a number of samples were also treated to the *peak-aged* (PA) temper, 24 h at 120ºC following the solution treatment and quenching, as the DSA/DP phenomena is largely suppressed in this temper. The choice of the NA temper, instead of the solution treated (ST), was made as the ST material is very unstable and the effects of temperature and deformation induced precipitation are harder to separate. Before testing, the samples were ground and polished to remove any effects of machining and surface roughness. The testing was performed in an INSTRON 8032 servo-hydraulic rig with a temperature chamber. The strain was measured using a 10 mm axial extensometer and a triangular fully reversed push-pull strain–time profile, with constant total strain amplitude and strain rate $1 \cdot 10^{-3}$ s^{-1}, was employed. The NA samples were deformed with a total strain amplitude of 0.6% and the PA with 0.8%, this to yield plastic strain amplitudes of 0.2% at half-life, at temperatures of –20, 20 and 60ºC. Inspired by the results on the influence of temperature on the monotonic properties of AA7030 [1-3,13], it was decided to perform tests at both lower and higher temperatures than ambient, namely –20°C, 20°C and 60°C.

Table 1: Composition of AA7030 in weight per cent.

Element	Al	Zn	Mg	Cu	Fe	Si
Wt.%	Bal.	5.2	1.1	0.3	0.18	0.06

3. Results and discussion

3.1. Cyclic stress–strain response

The hysteresis loops from the 20th cycle can be seen in Fig. 1, where the serrated yielding due to DSA is clearly visible at room temperature and 60°C. Figure 2 shows the stress amplitude, σ_a, as a function of number of cycles, N, and normalized fatigue life N/N_f. The results are discussed separately for the two tempers below.

3.1.1. Peak-aged temper

In the PA material, σ_a initially increases rapidly, reaching a maximum at approximately 30% of the fatigue life. After this, the amplitude decreases continuously until the on-set of rapid crack growth which can be determined from investigations of the plastic strain amplitude and peak-stress asymmetry (see later sections). The final catastrophic crack growth and fracture is very fast, occupying only a small fraction of the total fatigue life. The softening from peak stress amplitude is more pronounced at lower temperature. This leads to the observation that the stress amplitude at half-life is essentially temperature independent.

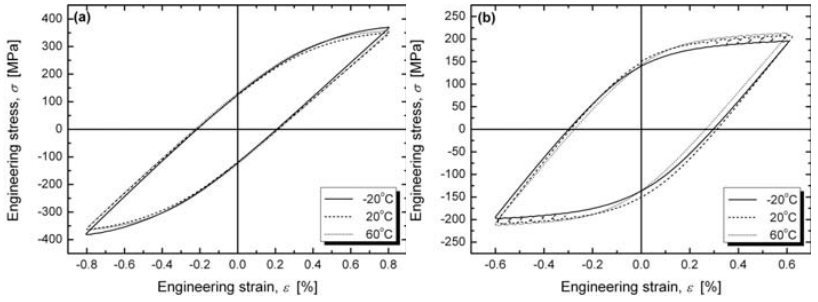

Fig. 1. Engineering stress–strain hysteresis loops from the 20th cycle of (a) PA and (b) NA samples deformed at different temperatures.

Most commercial 7000 aluminium alloys in the peak-aged (T6) condition exhibit initial cyclic hardening, followed by saturation [24-29]. In the present investigation, on the other hand, softening commences after about 20-30% of the fatigue life, progressively decreasing the stress amplitude until failure. Similar softening of peak- aged 7000 alloys has been observed before, *e.g.* [20,30], and is attributed to the shearable precipitates (GP-zones and small η') which act as the strengthening phases. When the particles are sheared, they lose some of the strength on the crystallographic slip plane. Further slip on the same plane is promoted, and localization of the strain into intense slip bands occurs. The dislocation structure will consist of slip bands with high dislocation density, acting as the plastic strain carriers, embedded in a matrix with low dislocation density [18,21,23]. The localization of strain in these bands results in the observed softening, as the flow stress in the bands decreases with the repeated cutting of the precipitates. The mechanism of softening of the bands in different precipitation hardened systems has been debated, but it has been argued that in 7000 alloys, the reversion of precipitates is responsible [23,31]. The occurrence of strain localization can be directly observed as slip bands on the sample surface, as seen in Fig. 3. The fact that softening is observed here, but not in most commercial alloys although the arguments should apply equally for other peak-aged 7000 materials, can be attributed to the large grain size, low Cu content and low concentration of dispersoid-forming elements.

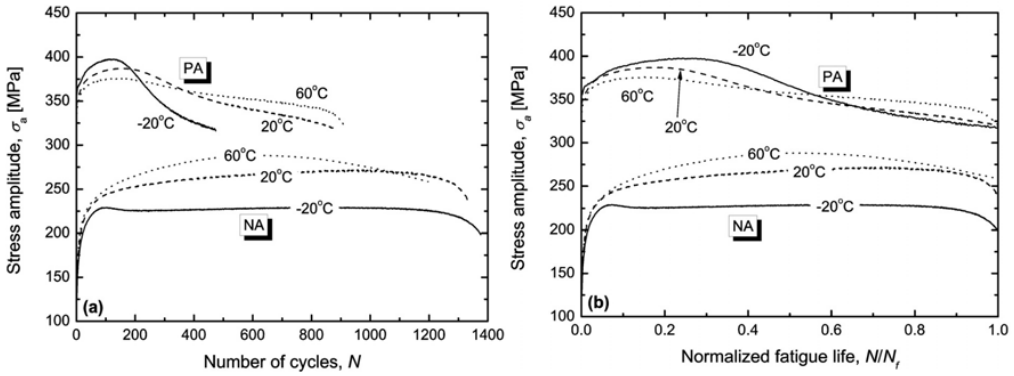

Fig. 2. (a) Cyclic stress response vs. number of cycles, N, and (b) vs. normalized fatigue lige N/N_f.

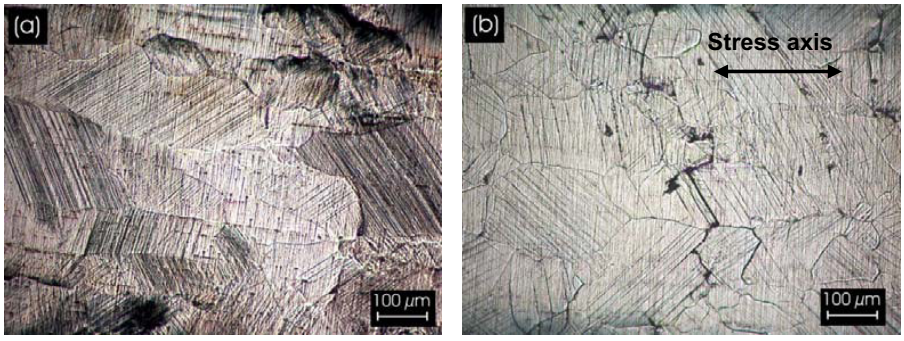

Fig. 3. Optical micrograph of the outer surface of (a) NA sample deformed at 60°C, and (b) PA sample deformed at room temperature.

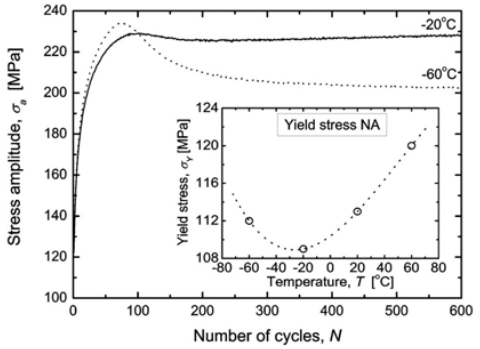

Fig. 4. Comparison of the initial part of the stress response curves for the NA temper deformed at -20 and -60°C with ε_a=0.6%. Inserted is the yield stress (σ_Y) measured as the 0.2% proof strength from the first cycle.

3.1.2. Naturally aged temper

Also the NA samples initially harden rapidly. However, the behavior after the initial transient, corresponding to roughly 10% of N_f, the behavior is distinctly temperature dependent. At 20 and 60°C, a period of slower hardening commences, where the hardening rate increases with temperature. This continues until the crack growth related softening begins. At –20°C on the other hand, the stress amplitude goes through a maximum at approximately 10% of the fatigue life, after which there is a decrease followed by a slow continuous increase until the crack growth comes to dominate.

In the NA temper, strain localization is observed at all test temperatures, but the density of the slip bands is much higher (Fig. 3(a)). The GP(I) zones in the NA state present much weaker obstacles to dislocation motion than the GP(II) and η' present in the PA material. Consequently, even though the particles are sheared by the moving dislocations so that slip bands are formed the strength difference between the bands and the matrix is small. As a result the localization is not as strong as in the PA condition [18,21], which is reflected in the high density of slip bands. Nevertheless, the presence of intense slip bands is expected to cause cyclic softening [21-23]. However, the present results show that at the two higher temperatures, 20°C and 60°C, the NA samples undergo cyclic hardening, and the rate of hardening increases with temperature. At –20°C, the samples actually soften after an initial period of hardening and then saturates. If the temperature is decreased further to –60°C (Fig. 4), the yield stress (0.2% proof stress from the first hysteresis loop) increases compared to the tests at –20°C, and the initial rapid hardening was more pronounced. The stress amplitude reaches a maximum, but the subsequent drop in σ_a is significantly more pronounced and following this, the amplitude slowly decreases for the remainder of the fatigue life.

These anomalous effects in the present case can be explained in terms of DSA and DP in the following way: The initial rapid hardening is a result of the generation and accumulation of dislocations [21]. Although DSA/DP can be expected to influence the behavior to some extent, i.e. increase the rate of hardening, the main mechanism is undoubtedly the increasing dislocation density and the resulting forest hardening. Somewhere around 10% of the fatigue life, according to Fig. 2, the dislocation structure is stabilized in the form of intense slip bands due to shearing of the GP zones, as explained above. At the lower test temperatures, –20°C and –60°C, there is a drop in the stress amplitude at this point, consistent with the expected cyclic softening. At –60°C, the diffusion rate is too low to allow an efficient DSA/DP process, and the softening continues progressively until failure, similar to the PA material. At –20°C, the increased diffusion rate in combination with the high dislocation density in the slip bands allow DSA/DP to commence. These effects balance the softening in the slip bands by the locking of dislocations and continuous precipitation of GP zones. Upon further temperature increases, the DSA/DP process is sufficiently fast to outweigh the softening mechanisms and there is a continuous stress amplitude increase. The hardening rate is higher at 60°C as the DSA/DP process is faster. However, as dislocation motion is hindered and the flow stresses are higher at this temperature, the initiation, growth and coalescence of micro-cracks are faster. Consequently, at approximately 50% of the fatigue life, the stress amplitude starts to decrease due to macroscopic crack growth. At 20°C, on the other hand, the crack initiation and growth are slower, and the hardening continues until late in the fatigue life.

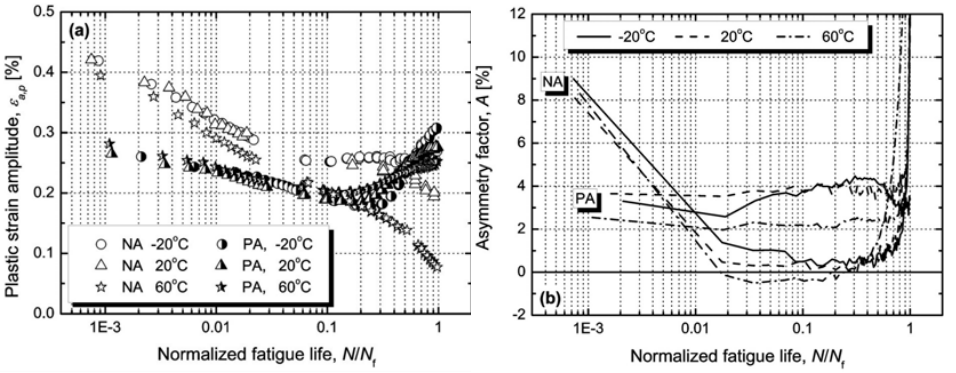

Fig. 5. (a) The plastic strain amplitude, $\varepsilon_{a,p}$, and (b)peak stress asymmetry factor, A, as a function of normalised fatigue life, N/N_f.

3.2. Plastic strain amplitude development

Another way to represent the cyclic hardening/softening behavior is to examine the development of the plastic strain amplitude, $\varepsilon_{a,p}$, with N/N_f, as shown in Fig. 5(a). The initial hardening can be seen as a decrease of $\varepsilon_{a,p}$, and it is obvious that the amount of cyclic hardening is greater in the NA temper. The behavior then essentially follows the development of the (inverse of the) stress amplitude in both tempers, where the softening after the peak stress amplitude in PA is seen as a continuous increase of $\varepsilon_{a,p}$, and the constant stress amplitude at –20°C and continuous hardening at 20°C in the NA temper is reflected in the curves in Fig. 5(a). The NA sample tested at 60°C, on the other hand, shows a somewhat different behavior. Even though σ_a decreases after $N/N_f = 0.5$, $\varepsilon_{a,p}$ continues to decrease until failure, presumably due to slow macroscopic crack growth which has started at approximately half-life, leading to changes in the hysteresis loop shape which comes through as an decreased plastic strain amplitude.

3.3. Peak stress asymmetry

The onset of crack growth can also be investigated by observation of the asymmetry factor, A, defined as

$$A = (|\sigma_c| - \sigma_t)/([|\sigma_c| + \sigma_t]/2) = -2\sigma_m/\sigma_a \quad (1)$$

where σ_t and σ_c are the true peak stresses, corrected for the Poisson effects, in tension and compression in a cycle and σ_m is the mean stress [25,32]. Consequently, a positive value of A in a given cycle indicates that the peak stress is higher in compression in that cycle, and vice versa. The development of A with N/N_f can be seen in Fig. 5(b). After an initial transient, A remains relatively constant with increasing number of cycles, indicating that both σ_t and σ_c undergo similar changes. At some point, the A values start to increase rapidly, i.e. the magnitude of σ_t decreases compared to σ_c, indicating macroscopic crack growth. In the PA temper, this occurs close to N/N_f=1, whereas rapid crack growth starts at roughly 70% of the fatigue life at –20°C and 20°C in NA, consistent with the development of σ_a. At 60°C, the on-set occurs much earlier, at N/N_f values of approximately 0.5, corresponding to the maximum in the stress amplitude, indicating much earlier growth of macroscopic cracks as compared to lower temperatures.

3.4. Internal and effective stresses

To further investigate the cyclic stress development, the decomposition of the stress into effective, σ_{eff}, and internal, σ_{int}, components was studied using the statistical approach (SAP) proposed by Polák *et al.* [33,34]. The results are presented in Fig. 6. It is considered that the internal stress, σ_{int}, is a function of the long-range stress fields built up in the material and is therefore purely athermal. The effective stress, σ_{eff}, on the other hand, is related to the stresses on the dislocations imposed by the strains in the material, and has both a thermal and an athermal component. Using this, and the presence of DSA/DP during deformation, it is possible to hypothesize regarding the development of the stress components with cycling as follows:

In the PA temper, σ_{int} increases initially as the dislocation density is built up. Early in the deformation, the dislocation structure develops and σ_{int} decreases, whereas the effective stress continues to increase due to the dislocation-dislocation interactions. As the precipitates are sheared, the dislocation structure takes the form of intense slip bands, corresponding to a stable value of the long-range stresses. At this point, σ_{eff} decreases as the planar deformation in the slip bands decreases the interaction between mobile and forest dislocations.

The behavior of the NA material is different. Initially, both σ_{eff} and σ_{int} increase as the dislocation density increases. After about 10% of the fatigue life, the banded dislocation structure takes form and σ_{int} starts to decrease. σ_{eff}, on the other hand, continues to increase as the DP continuously increases the glide resistance in the bands. The effect of the temperature can be clearly seen: an increased temperature, corresponding to more efficient DP, leads to higher values of σ_{eff} and this behavior controls the stress amplitude. The internal stress on the other hand decreases with temperature.

Bath and Laird [19] argued that in precipitation hardened poly-crystals a part of the effective stress, approximately equal in magnitude to the internal stress, should develop with accumulated plastic strain in the same manner as the internal stress and that the effective stress component due to the presence of precipitates is given by $\sigma_{eff,prec}=\sigma_{eff}-\sigma_{int}$. Applying this in the present case leads to initially negative values of $\sigma_{eff,prec}$ in the NA temper. Assuming that the fraction of σ_{eff} *not* connected to the precipitates is larger than proposed by Bath and Laird, so that $\sigma_{eff,prec}$ is positive, the precipitate effects according to this approach can be seen in Fig. 7 (note the relative scaling of the ordinate in Fig. 7). During the initial transient, the internal stress development is important due to the rapid accumulation of dislocations, but after some few percent of the fatigue life, $\sigma_{eff,prec}$ essentially follows the development of the stress amplitudes, confirming that the stress–strain response in both tempers is essentially controlled by the effective stresses associated with the precipitate–dislocation interactions.

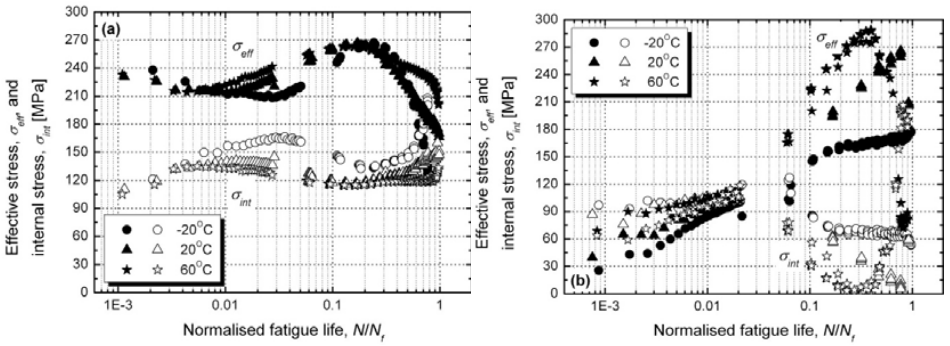

Fig. 6. Development of the effective, σ_{eff}, and internal, σ_{int}, stress components with normalised fatigue life N/N_f in (a) for PA samples cyclically deformed with ε_a=0.8% and NA samples with ε_a=0.6%, at different temperatures.

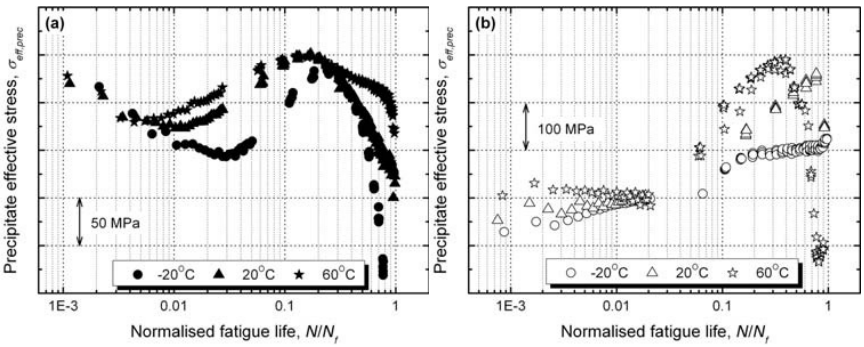

Fig. 7. The development of the part of the effective stress associated with the precipitates in (a) PA and (b) NA temper. The absolute magnitudes of the stresses are not known (see the text in the discussion) and the scaling of the ordinate is therefore relative.

4. Conclusions

The stress–strain response of the NA temper is determined by the combination of strain localisation and concurrent dynamic strain ageing (DSA) and dynamic precipitation (DP). At temperatures where DSA/DP is largely suppressed, initial rapid hardening followed by an abrupt drop in the stress amplitude and subsequent saturation or slow softening, is observed. At higher temperatures, DSA/DP outweighs the inherent slip band induced softening, and the stress amplitude increases up to the point of catastrophic crack growth. The stress levels increased with temperature due DSA and DP, and the occurrence of these phenomena could be used to explain the evolution of the internal and effective stresses derived from the hysteresis loops.

In the PA temper, where DSA/DP are suppressed due to solute depletion, the samples initially harden rapidly to a peak stress and subsequently soften due to microstructural effects until the onset of final catastrophic crack growth. The behavior can be explained in terms of strain localization due to precipitate shearing in combination with a large grain size and the absence of dispersoid-forming elements.

References

[1] Hörnqvist M, Karlsson B. Dynamic strain ageing effects in an extruded AA7030 alloy subjected to tensile deformation. In: *Proceedings of The 11th Int. Conf. on Fracture*, Turin, Italy, 2005.
[2] Hörnqvist M, Karlsson B. Temperature and strain rate effects on the dynamic strain ageing of AA7030. *Mat. Sci. Forum* 2006;**519-521**: 883.
[3] Hörnqvist M, Karlsson B.Temperature and strain rate dependence of the dynamic strain ageing effect in an Al-Zn-Mg alloy. *Mat. Sci. Tech.* 2006;**22**:213.
[4] Fjeldly A, Søreng A, Roven HJ. Shear localization in solution heat treated AlZnMg alloys. *Mat. Sci. Eng.* 2001;**A300**:165.
[5] Shabadi R, et al. Dynamic plasticity in solid solution: Observations and quantification. *La Metallurgia Italiana* 2002;**7-8**:21.
[6] Shabadi R, et al. Propagative plasticity in commercial aluminium alloys. *Trans. Indian Inst. Metals* 2004;**57**:61.
[7] Shabadi R, et al. Assessing formability of sheet metals through advanced tensile and laser speckle analysis. *Mat. Sci. Forum* 2002;**396-402**:1623.
[8] Shabadi R, et al. Characterisation of PLC band parameters using laser speckle technique. *Mat. Sci. Eng.* 2004;**A364**:140.
[9] Hörnqvist M, Karlsson B. Effect of heat treatment on the strain hardening behaviour of an Al-Zn-Mg alloy. *Int. J. Mat. Res.* 2009:**100**:1574.
[10] Deschamps A, et al. Anomalous strain hardening behaviour of a supersaturated Al-Zn-Mg alloy. *Mat. Sci. Eng.* 1997;**A234-236**:477.
[11] Deschamps A, et al. Low temperature dynamic precipitation in a supersaturated Al-Zn-Mg alloy and related strain hardening. *Phil. Mag. A* 1999;**79**:2485.
[12] Deschamps A, et al. In-situ small-angle X-ray scattering study of dynamic precipitation in an Al-Zn-Mg-Cu alloy. *Phil. Mag.* 2003;**83**:677.
[13] Hörnqvist M, Karlsson B.Temperature and strain rate effects on the work hardening behaviour of AA7030. In: Hirsch J, Skrotzki G, Gottstein G, editors. *Proceedings of the 11th Int. Conf. on Aluminium Alloys.* Aachen, Germany, 2008:**2**:1498.
[14] Deschamps A, et al. Strain hardening rate in relation to microstructure in precipitation hardening materials. *J. Phys. IV* 2000;**10**:151.
[15] Pink E, Webernig WM. Precipitation during serrated flow in AlZn5Mg1. *Acta Metall.* 1987;**35**:127.
[16] Christ HJ, et al. The role of microstructural processes in the application of the incremental step test to determine the cyclic stress-strain curve of an alumnium alloy. In: Rie KT, et al., editors. *Proceedings of the 3rd Int. Conf. on Low-Cycle Fatigue and Elasto-Plastic Behaviour of Materials.* Berlin, Germany, 1992:100.
[17] Laird C, et al. The cyclic stress-strain response of precipitation hardened Al-15 wt.% Ag alloy. *Mat. Sci. Eng.* 1978;**32**:137.
[18] Clark JB, McEvily AJ. Interaction of dislocations and structures in cyclically strained aluminum alloys. *Acta Metall.* 1964;**12**:1359.
[19] Bhat SP, Laird C. High temperature cyclic deformation of precipitation hardened alloy—II. Fully coherent precipitates. *Acta Metall.* 1979;**27**:1873.
[20] Hörnqvist M, B. Karlsson B. Influence of heat treatment on the cyclic deformation properties of aluminium alloy AA7030. *Mat. Sci. Eng.* 2008;**A479**:345.
[21] Calabrese C, Laird C. Cyclic stress-strain response of two-phase alloys Part I. Microstructures containing particles penetrable by dislocations. *Mat. Sci. Eng.* 1974;**13**:141.
[22] Calabrese C, Laird C. High strain fatigue fracture mechanisms in two phase alloys. *Metall. Trans.* 1974;**5A**:1785.
[23] Wilhelm M. The cyclic stress-strain behaviour of age-hardened Cu-Co and Al-Zn-Mg alloy single crystals. *Mat. Sci. Eng.* 1981;48:91.
[24] Laird C. The general cyclic stress-strain response of aluminum alloys. *ASTM STP*. 1977;**637**:3.
[25] Meininger JM, Dickerson SL, Gibeling JC. Observation of tension/compression asymmetry in the cyclic deformation of aluminum alloy 7075. *Fatigue Fract. Engng. Mater. Struct.* 1996;**19**:85.
[26] Mercer ME, Dickerson SL, Gibeling JC. Cyclic deformation of dispersion-strengthened aluminum alloys. *Mat. Sci. Eng.* 1995,**A203**:46.
[27] Li P, Marchand NJ, Ilschner B. Crack initiation mechanisms in low cycle fatigue of aluminium alloy 7075 T6. *Mat. Sci. Eng.* 1989;**A119**:41.
[28] Sanders TH, Starke EA. The relationship of microstructure to monotonic and cyclic straining of two age hardening aluminum alloys. *Metall. Trans.* 1976;**7A**:1407.
[29] Sanders TH, Starke EA. The effect of grain refinement on the low cycle fatigue behavior of an Aluminum-Zinc-Magnesium-(Zirconium) alloy. *Mat. Sci. Eng.* 1977;**28**:53.

[30] Lin FS, Starke EA. The effect of copper content and degree of recrystallization on the fatigue resistance of 7XXX type aluminum alloys I. Low cycle corrosion fatigue. *Mat. Sci. Eng.* 1979;**39**:27.
[31] Stubbington CA, Forsyth PJE. Some observations on microstructural damage produced by fatigue of an aluminium-7.5% zinc-2.5% magnesium alloy at temperatures between room temperature and 250°C. *Acta Metall.* 1966;**14**:5.
[32] Ma BT, et al. Asymmetry behavior between tension and compression in the cyclic deformation of copper single crystals and other ductile metals. *Mat. Sci. Eng.* 1990;**A129**:197.
[33] Polák J, Klesnil M. The hysteresis loop 1. A statistical theory. *Fatigue Fract. Engng. Mater. Struct.* 1982;**5**:19.
[34] Polák J, Klesnil M, Helesic J. The hystersis loop 2. An analysis of the loop shape. *Fatigue Fract. Engng. Mater. Struct.* 1982;**5**:33.